Impact of Targeted Winter Storm Reconnaissance Dropwindsonde Data on Mid-latitude Numerical Weather Predictions

Thomas M. Hamill[1], Fanglin Yang[2,3], Carla Cardinali[4],

and Sharanya J. Majumdar[5]

[1] *NOAA Earth System Research Lab, Physical Sciences Division, Boulder, Colorado*

[2] *I.M. Systems Group, Inc., Rockville, Maryland*

[3] *NOAA/NCEP Environmental Modeling Center, College Park, Maryland*

[4] *European Centre for Medium Range Weather Forecasts, Reading, England*

[5] *Rosenstiel School of Marine and Atmospheric Science, University of Miami, Florida.*

Submitted to *Monthly Weather Review as an expedited contribution*

18 October 2012

Corresponding author address:

Dr. Thomas M. Hamill

NOAA Earth System Research Lab, Physical Sciences Division

R/PSD1, 325 Broadway

Boulder, Colorado, USA 80305

tom.hamill@noaa.gov, (303) 497-3060

Abstract

The impact of data from the 2011 Winter Storm Reconnaissance (WSR) program on numerical weather forecasts was assessed. Parallel sets of analyses and deterministic 120-h numerical forecasts were generated using the ECMWF 4D-Var and Integrated Forecast System. One set of analyses was generated with all of the normally assimilated data plus WSR targeted dropsonde data, the other with only the normally assimilated data. Forecasts were then generated from the two analyses. The comparison covered the period from 10 January 2011 to 28 March 2011, during which 98 flights and 776 total dropsondes were deployed from four different air bases in the Pacific basin and US. The dropsondes were deployed in situations where guidance indicated the potential for high-impact weather and/or the potential for large subsequent forecast errors, and downstream target locations where high-impact weather was expected. Forecast errors around the target verification regions were evaluated using an approximation to the total-energy norm. Precipitation forecasts were also evaluated over the eastern US using the equitable threat score and bias.

Forecast impacts were generally neutral and thus smaller than reported in previous studies, most from ~ 10 years ago, perhaps because of the improved forecast and assimilation system and the somewhat denser observation network. Target areas may also have been under-sampled in this study. The neutral results from 2011 suggest that it may be more beneficial to explore other targeted observation concepts for the mid-latitudes, such as assimilation of a denser set of cloud-drift winds and radiance data in dynamically sensitive regions.

1. **Introduction**

Since the mid-1990s, supplementary "targeted" atmospheric observations have been deployed in relative data voids in the extratropics, such as the open ocean under cloud shields. The additional data were collected in an attempt to improve the operational numerical weather prediction (NWP) of potential high-impact weather events through assimilation of these extra data. The most extensive use of targeted observations in the extratropics has been through the annual National Oceanographic and Atmospheric Administration (NOAA) Winter Storm Reconnaissance (WSR) program, which has been operational since 2001. During each day of WSR, NOAA forecasters identify weather systems that may impact the contiguous United States and Alaska up to a week in advance and estimate the uncertainty associated with the forecast of each system. They pick a "target verification location" where the high-impact weather is centered and then assign a low, medium or high priority to each case. The Ensemble Transform Kalman Filter technique (ETKF, Bishop et al. 2001, Majumdar et al. 2002a) is then used to identify potential upstream "sensitive areas," primarily over the northern Pacific Ocean, in which the assimilation of targeted observations is expected to maximally improve the subsequent forecast of the weather event in question. Selecting from a pre-defined series of flight tracks of NOAA Gulfstream IV (G-IV) and United States Air Force C-130 aircraft carrying Global Positioning System (GPS) dropwindsondes, a flight request is submitted two days prior to the actual flight deployment. These data are then assimilated into operational global NWP systems. For more comprehensive details of the field of targeted observations, the interested reader is referred to review articles by Langland (2005) and Majumdar et al. (2011).

The decision to implement WSR in NOAA's operations was based on the promising results of the NORPEX-98 and experimental WSR field campaigns in 1999 and 2000, in which verification studies found that the majority of lower-resolution targeted forecasts were significantly improved (Langland et al. 1999; Szunyough et al. 2000, 2002). Additionally, evaluations of the ETKF had demonstrated that it can efficiently and accurately predict the reduction in the error variance of 1-3 day forecasts due to targeted observations, prior to each deployment (Majumdar et al. 2001, 2002a). The broader-scale aspects of ETKF targets were largely found to agree with those of adjoint-based techniques such as singular vectors (Majumdar et al. 2002b). Recent studies have demonstrated the utility of the ETKF out to 7 days, with sensitive areas traceable as far upstream as Japan (Sellwood et al. 2008; Majumdar et al. 2010). Consequently, WSR aircraft have been stationed in Japan since 2009 to collect targeted observations, in an attempt to improve medium-range forecasts.

Since the advent of WSR, much has changed in numerical weather prediction (NWP), and there are concerns in the community that previous optimistic results from over a decade ago may not be replicable today. Forecast models are now much higher in resolution and incorporate better physical parameterizations, thus producing better prior forecasts for the data assimilation. Additionally, advanced data assimilation methods such as 4-dimensional variational assimilation (4D-Var) are now operational at almost all NWP centers, reducing analysis errors further. The observing network is also more extensive than it was a decade ago, as is the assimilation of satellite data in operational NWP systems. Finally, there is concern that the areas that need to be sampled may be so prohibitively large that ~10-20 additional dropwindsondes may be inadequate (Langland 2005).

88 WSR has not recently performed careful data denial experiments with a modern
89 data assimilation and forecast system, testing the forecast impact with and without the
90 targeted observations. This paper reports on an attempt to perform such an experiment
91 using 2011 WSR data and the European Centre for Medium-Range Weather Forecasts
92 (ECMWF) assimilation and forecast system. The hypothesis to be tested is as follows:
93 given a reasonably selected set of targeted observations, forecasts that incorporate the
94 assimilation of these additional observations will be significantly more skillful than
95 forecasts that do not, and the extra observations will be especially important for cases with
96 anticipated high-impact weather. Further, we hypothesize that the impact of the targeted
97 observations will be larger in specific downstream 'verification regions' focused on the
98 expected area with high-impact weather and that the impact will be smaller when
99 evaluated over continental-sized areas.

100 **2. Targeted data, model, and data assimilation system**

101 The WSR program is coordinated each year by the NOAA National Centers for
102 Environmental Prediction (NCEP), who have kept a log of daily flight requests, and the
103 forecast lead time, verification time, target verification locations, and the priority of each
104 forecast case at http://www.nco.ncep.noaa.gov/pmb/sdm_wsr/ from 2003 to the present.
105 In 2011, a total of 776 dropsondes were deployed by the NOAA and USAF aircraft which
106 took off from four different air bases (Anchorage, Biloxi, Yokota and Honolulu). During the
107 2011 WSR period there were 22 high-priority cases, 62 medium-priority cases, and 14 low-
108 priority cases. The forecast lead time associated with a given target verification for an
109 event ranged from +12 hours to +120 hours post assimilation. The lead time was

110 calculated as the difference between the forecast target verification time and the
111 initialization time. A plot of the target verification locations during the 2011 WSR
112 campaign from 10 January 2011 through 26 March 2011 is shown in Fig. 1, including the
113 assigned priority for each target and the forecast lead time.

114 Two parallel forecast experiments were carried out using the ECMWF's 4D-Var data
115 assimilation system and global weather forecast model for the period from 9 January 2011
116 through 28 March 2011. The first set included the 2011 WSR dropwindsonde data
117 ("CONTROL") and the second set excluded the dropwindsonde data ("NODROP"). For both
118 assimilation cycles, $\sim 10^7$ other observations were assimilated in both CONTROL and
119 NODROP experiments, i.e., the full data stream normally assimilated at ECMWF. In
120 particular, the surface-based observations were SYNOP (measuring surface pressure, 10-m
121 winds, and 2-m relative humidity), DRIBU (buoys measuring surface pressure and 10-m
122 winds), radiosonde (measuring temperature, winds, and humidity profiles), aircraft
123 (measuring temperature and wind profile), profilers, and PIBAL (measuring wind profiles).
124 From the geostationary platforms (Meteosat, GOES, MTSAT, and MODIS), two different
125 observation types were assimilated, atmospheric motion vectors (retrieved wind profiles)
126 and infrared sounder radiances. From the polar orbiting platforms, the following were
127 assimilated: AMSU-A, AMSU-B, MHS and MSG (all measuring microwave-sounder radiance),
128 IASI, AIRS and HIRS (measuring infrared-sounder radiance), SSMI, SSMIS, TMI, AMSR-E
129 (microwave-imager radiance), ASCAT and ERS (retrieved wind product from microwave
130 scatterometer backscatter coefficients), and GPS-Radio Occultation (measuring radio
131 occultation bending angle). Both CONTROL and NODROP were cycled continuously for the
132 entire campaign period, whether the targeted dropwindsonde data were available or not.

When targeted observations were taken, subsequent deterministic forecasts were produced to +120 hours lead. In all cases, the CONTROL analysis was used for verification, which may bias the results at the early leads slightly to favor the CONTROL forecasts. For both cycles, ECMWF used version 37r2 of their Integrated Forecast System (IFS; www.ecmwf.int/products/data/operational_system/evolution/evolution_2011.html). The resolution of the forecast model was T511 (~0.35-degree grid spacing on reduced linear Gaussian grid), with 91 vertical levels The data assimilation, ECMWF's 4D-Var system, uses a full nonlinear trajectory at T511 L91 (outer loop) and a linearized model (Janiskova and Lopez 2012) at the resolutions T159, T159, and T255 for the three minimization inner loops, respectively. The ECMWF 4D-Var system also used background error variances "of the day" as estimated from the low resolution (T399 L91 outer loop, linearized T159 inner loops) ensemble data assimilation (Bonavita et al. 2010).

3. Description of norms used to evaluate forecast impact.

The impact of assimilating the dropwindsonde data on ECMWF forecast skill was calculated using a crude approximation to the commonly used dry total-energy norm. Let **u** represent a gridded state vector of forecast minus analysis differences for the *u*-wind component. Similarly, **v**, **t**, and **p** represent fields of differences in *v*-wind, temperature, and surface pressure. Then the error *E* for a domain A was

151
$$E = \left[\frac{1}{2} \int_A \left(\begin{array}{l} \frac{1}{4}\left(\mathbf{u}_{250}^2 + \mathbf{v}_{250}^2 + \frac{c_p}{T_r}\mathbf{t}_{250}^2 \right) + \\ \frac{1}{4}\left(\mathbf{u}_{500}^2 + \mathbf{v}_{500}^2 + \frac{c_p}{T_r}\mathbf{t}_{500}^2 \right) + \\ \frac{1}{4}\left(\mathbf{u}_{850}^2 + \mathbf{v}_{850}^2 + \frac{c_p}{T_r}\mathbf{t}_{850}^2 \right) + \\ \frac{1}{4}\left(\mathbf{u}_{10m}^2 + \mathbf{v}_{10m}^2 + \frac{c_p}{T_r}\mathbf{t}_{2m}^2 \right) + R_d T_r \left(\frac{\mathbf{p}}{P_r} \right)^2 \end{array} \right) \right]^{1/2}, \quad (4)$$

152 where the state vector subscripts denote the constant pressure level (250 hPa, 500 hPa,
153 850 hPa) or the height above ground (10 m, 2 m). c_p represents the specific heat content of
154 dry air at constant pressure (= 1004 J K^{-1} kg^{-1}), T_r is the reference temperature (= 300K),
155 R_d is the gas constant for dry air (= 287 J K^{-1} kg^{-1}) , and P_r is the reference pressure (= 1000
156 hPa). The integral sign indicates that the error was integrated and averaged over the
157 domain A, accounting for latitudinal variations in grid spacing. The domain A will differ
158 with different tests. This approximation to the total-energy norm provides a bit extra
159 weight to near-surface fields, which may be desirable given their greater societal relevance.
160 The impact was first evaluated in relatively confined verification regions, +/- 10 degrees
161 latitude and longitude around the verification location of interest at the specific lead time
162 of the target forecast, which may change from +12 h to +120 h depending on the case day.
163 This size of verification region was chosen to closely resemble the 10-degree radius region
164 used in previous WSR evaluations. Next, similar statistics were computed within a larger
165 Pacific/North American (PNA) region covering North America and adjacent coastal waters
166 (20° N - 75° N, 180° E - 320° E). Equitable threat scores and bias (Wilks 2006, eqs. 7.18
167 and 7.10, respectively) were also computed over the contiguous United States (CONUS).

168 Precipitation forecasts were evaluated at stations, bilinearly interpolating the forecast data
169 to gauges within the CONUS that report 24-h accumulated amounts.

170 **4. Forecast impact.**

171 Figure 2 provides a comparison of the forecast errors for NODROP vs. CONTROL.
172 Panel (a) provides a scatterplot of the data, with the CONTROL errors on the abscissa and
173 NODROP errors on the ordinate. There is a symbol associated with each case, with
174 different symbols for the different lead times. Cases above the diagonal line indicate cases
175 with some improvement from the assimilation of dropsonde data. Panel (b) provides
176 another way of viewing the differences, this time as a scatterplot as a function of the
177 forecast lead time. Different symbols indicate the different priorities assigned to the cases.
178 The solid line provides the mean difference for each lead time, and the dashed line
179 indicates one standard deviation. While there are some slight positive differences, there
180 are about as many negative differences. This 2011 data do not support the hypothesis that
181 the differences with vs. without targeted observations are statistically significant in the
182 localized verification region. From visual inspection, there is no obvious relationship
183 between the priority of the case and the impact; in fact, the forecast impact of high-priority
184 cases appear well mixed with the ones of medium- and low-priority cases. Objective
185 statistics as a function of the priority were not calculated because of the small sample sizes.
186 Figure 3 provides the same type of information, but here over the PNA region. The forecast
187 errors averaged over this larger area are also very similar between CONTROL and NODROP.
188 A different forecast skill index such as the anomaly correlation (e.g, 500 hPa time series,
189 not shown) also showed a similar lack of impact.

We also examined the precipitation equitable threat scores and biases for both +24 to +48 h accumulations (Fig. 4) and for +48 to +72 h accumulations (Fig. 5) over the contiguous US. The differences are not statistically significant.

5. Discussions and conclusions.

This study has briefly summarized the impact from the assimilation of targeted observations from the 2011 Winter Storms Reconnaissance Program. Parallel cycles of ECMWF's data assimilation and deterministic forecasts were conducted, including and excluding the targeted observations with the rest of the regularly assimilated data. Differences were not statistically significant. The 2011 results do not support the hypothesis that differences between forecasts with and without these assimilated dropsondes are statistically significantly improved in the localized verification region. There may be several reasons for the lack of impact noted here. Observing systems have gotten denser in the ~10 years since the last systematic, peer-reviewed studies including the Pacific basin, with more cloud-track winds, aircraft, satellite radiance, and radio occultation data from global positioning satellites. Many other observing systems may now have relatively limited impact were they evaluated in a similar observing systems experiment. Data assimilation and forecast systems have improved as well. Additionally, it is recognized that a handful of dropsondes will incompletely sample the initial sensitive area due to limitations on how far and where the plane deploying them can fly.

It might be possible that data from different years or seasons has a different impact. Recently, R. Gelaro (personal communication, 2012) found that using NASA's adjoint sensitivity method and their assimilation system (Gelaro et al. 2010), the assimilated

dropsonde data had a large positive impact on a global measure of 24-h forecast error in several cases during WSR 2012. However, these impact results have not yet been measured with an observing system experiment such as were conducted here.

For the foreseeable future, the global observing network will continue to have regions with relatively sparse in-situ data. The challenge will be to supplement the existing network in the most cost-effective manner. WSR plane flights into the central Pacific are typically quite expensive, with fuel costs alone typically in the tens of thousands of US dollars. In a comparison study of observation impacts in three forecast systems, Gelaro et al. (2010) showed that only a small majority of the total number of assimilated observations actually improve the 24-h forecast, with much of the improvement coming from a large number of observations having relatively small individual impacts. Those authors argue that accounting for this behavior may be especially important when considering strategies for deploying adaptive components of the observing system. Given this and the results of the present study, we suggest refocusing the targeting concept to use available resources such as high-resolution satellite data. Sensitive areas, whether they are determined by forecasters or by objective algorithms, can potentially be monitored more closely by turning on the rapid-scan feature on geostationary satellites and then assimilating a denser network of motion vectors, such as in Berger et al. (2011). Perhaps a denser network of radiance data can be assimilated in sensitive regions (Bauer et al. 2011).

Acknowledgments:

Members of the THORPEX Data Assimilation and Observing Systems Committee are thanked for providing guidance on the experimental design and the methods for verification and for informal reviews of this manuscript. Publication of this article was supported with a grant from the NOAA THORPEX program, managed by John Cortinas, director of the Office of Weather and Air Quality.

References

Bauer, P., R. Buizza, C. Cardinali, and J.-N. Thepaut, 2011: Impact of singular vector based satellite data thinning on NWP. *Quart. J. Royal Meteor. Soc.*, **137**, 277-285.

Berger, H., R. H. Langland, C. S. Velden, C. A. Reynolds, and P. M. Pauley, 2011. Impact of Enhanced Satellite-Derived Atmospheric Motion Vector Observations on Numerical Tropical Cyclone Track Forecasts in the Western North Pacific during TPARC/TCS-08. *J. Applied Meteor. Clim.*, **50**, 2309-2318.

Bishop, C. H., B. J. Etherton, and S. J. Majumdar, 2001: Adaptive sampling with the Ensemble Transform Kalman Filter. Part I: Theoretical aspects. *Mon. Wea. Rev.*, **129**, 420-436.

Bonavita, M., L. Raynaud, and L. Isaksen, 2010: Estimating background error variances with the ECMWF ensemble of data assimilation: the effect of ensemble size and day-to-day variability. *Quart. J. Royal Meteor. Soc.*, **137**, 423-434.

Gelaro, R., R. H. Langland, S. Pellerin, and R. Todling, 2010: The THORPEX observation impact intercomparison experiment. *Mon. Wea. Rev.*, **138**, 4009-4025.

Janiskova, M., and P. Lopez, 2012. Linearized physics for data assimilation at ECMWF. ECMWF Technical Memorandum 666. Available at http://www.ecmwf.int/publications/library/do/references/show?id=90382

Langland, R. H., Z. Toth, R. Gelaro, I. Szunyogh, M. A. Shapiro, S. Majumdar, R. Morss, G. D. Rohaly, C. Velden, N. Bond, and C. Bishop, 1999: The North-Pacific Experiment

(NORPEX-98) Targeted observations for improved North American Weather Forecasts. *Bull. Amer. Meteorol. Soc.*, **80**, 1363-1384.

Langland, R. H., 2005: Issues in targeted observing. *Quart. J. Royal Meteor. Soc*., **131**, 3409-3425.

Majumdar, S. J., C. H. Bishop, B. J. Etherton, I. Szunyogh and Z. Toth, 2001: Can an ensemble transform Kalman filter predict the reduction in forecast-error variance produced by targeted observations? *Quart. J. Royal Meteor. Soc*., **127**, 2803–2820.

Majumdar, S. J., C. H. Bishop, B. J. Etherton and Z. Toth, 2002a: Adaptive sampling with the ensemble transform Kalman filter. II: Field program implementation. *Mon. Wea. Rev*., **130**, 1356–1369.

Majumdar, S. J., C. H. Bishop, R. Buizza and R. Gelaro, 2002b: A comparison of ensemble-transform Kalman-filter targeting guidance with ECMWF and NRL total-energy singular vector guidance. *Q. J. R. Meteorol. Soc*., **128**, 2527–2549.

Majumdar, S. J., K. J. Sellwood, D. Hodyss, Z. Toth and Y. Song, 2010: Characteristics of target areas selected by the Ensemble Transform Kalman Filter for medium-range forecasts of high-impact winter weather. *Mon. Wea. Rev.*, **138**, 2803-2824.

Majumdar, S. J., S. D. Aberson, C. H. Bishop, C. Cardinali, J. Caughey, A. Doerenbecher, P. Gauthier, R. Gelaro, T. M. Hamill, R. H. Langland, A.C. Lorenc, T. Nakazawa, F. Rabier, C. A. Reynolds, R. Saunders, Y. Song, Z. Toth, C. Velden, M. Weissmann, and C.-C. Wu, 2011: Targeted observations for improving numerical weather prediction: an overview. World Weather Research Programme/THORPEX Publication No. 15, 37

pp. Available at http://www.wmo.int/pages/prog/arep/wwrp/new/documents/THORPEX_No_15.pdf.

Sellwood, K. J., S. J. Majumdar, B. E. Mapes and I. Szunyogh, 2008: Predicting the influence of observations on medium-range winter weather forecasts. *Quart. J. Roy. Meteor. Soc.*, **134**, 2011-2027.

Szunyogh, I., Z. Toth, S. Majumdar, R. Morss, B. Etherton, and C. Bishop, 2000: The effect of targeted dropsonde observations during the 1999 Winter Storm Reconnaissance program. *Mon. Wea. Rev.,* **128**, 3520-3537.

Szunyogh, I., Toth, Z., Zimin, A. V., Majumdar, S. J. and Persson, A. 2002: Propagation of the effect of targeted observations: The 2000 Winter Storm Reconnaissance Program. *Mon. Wea. Rev.,* **130**, 1144–1165.

Wilks, D. S., 2006: *Statistical Methods in the Atmospheric Sciences*. Academic Press, 627 pp.

Figure captions.

Figure 1: Scatterplot of the target central locations. Triangles denote low-priority cases, filled circles for medium-priority, squares for high priority. The forecast lead time is denoted by the color of the symbol, indicated by the legend on the left-hand side.

Figure 2. (a) Scatterplot of forecast errors for the target verification regions, CONTROL (x-axis) vs. NODROP (y-axis). Data for the different forecast lead times are denoted by different symbols, as shown in the figure legend. (b) Differences of RMS errors in the energy norm between the NODROP and CONTROL experiments. Bold line indicates the mean difference for each lead time and dashed lines indicate +/- one standard deviations around the mean for the samples at a given lead time, averaged over all of the low, medium, and high-priority cases.

Figure 3: As in Fig. 2, but for the PNA region (20° N - 75° N, 180° E - 320° E).

Figure 4: Equitable threat score and bias score for 24-hour accumulated precipitation from forecast hours +24 to +48 verified over the contiguous US. Top panels provide the scores, and bottom panels provide the difference (solid lines) between the NODROP and CONTROL experiments and 95% confidence intervals (bars) based on 1000 realizations of Monte-Carlo tests.

Figure 5: As in Fig. 4, but for 24-hour accumulated precipitation from forecast hours +48 to +72.

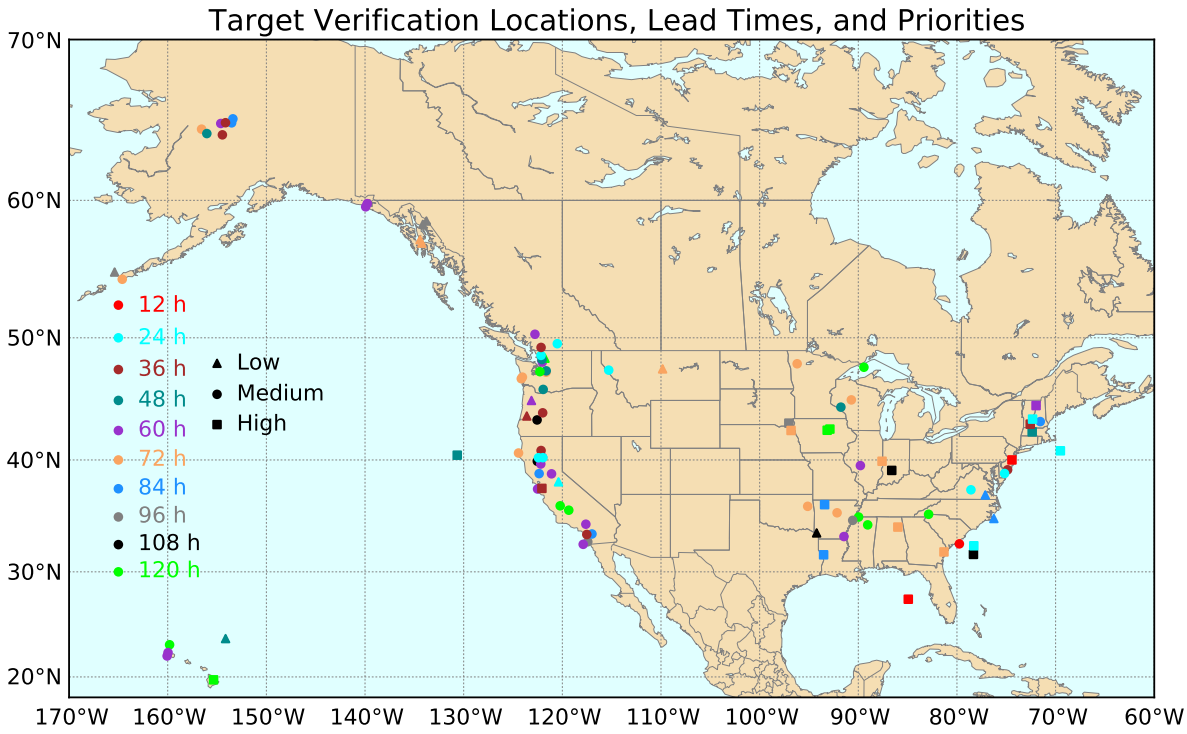

315

316 **Figure 1**: Scatterplot of the target central locations. Triangles denote low-priority cases, filled
317 circles for medium-priority, squares for high priority. The forecast lead time is denoted by the color
318 of the symbol, indicated by the legend on the left-hand side.

319

320

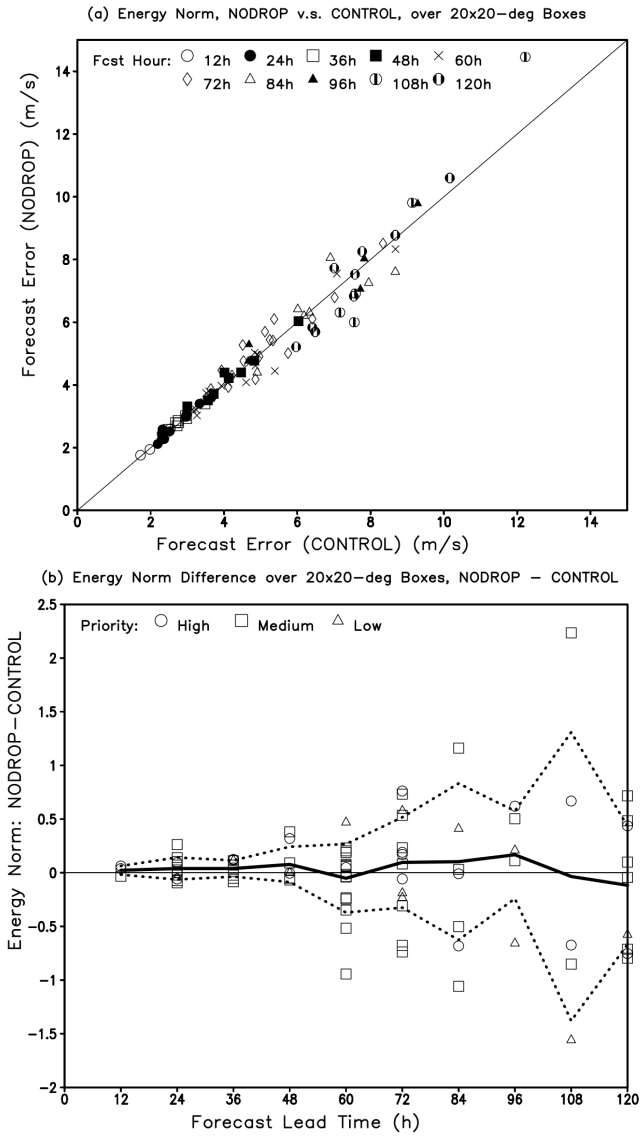

Figure 2. (a) Scatterplot of forecast errors for the target verification regions, CONTROL (x-axis) vs. NODROP (y-axis). Data for the different forecast lead times are denoted by different symbols, as shown in the figure legend. (b) Differences of the energy norm between the NODROP and CONTROL experiments. Bold line indicates the mean difference for each lead time and dashed lines indicate +/- one standard deviations around the mean for the samples at a given lead time, averaged over all of the low, medium, and high-priority cases.

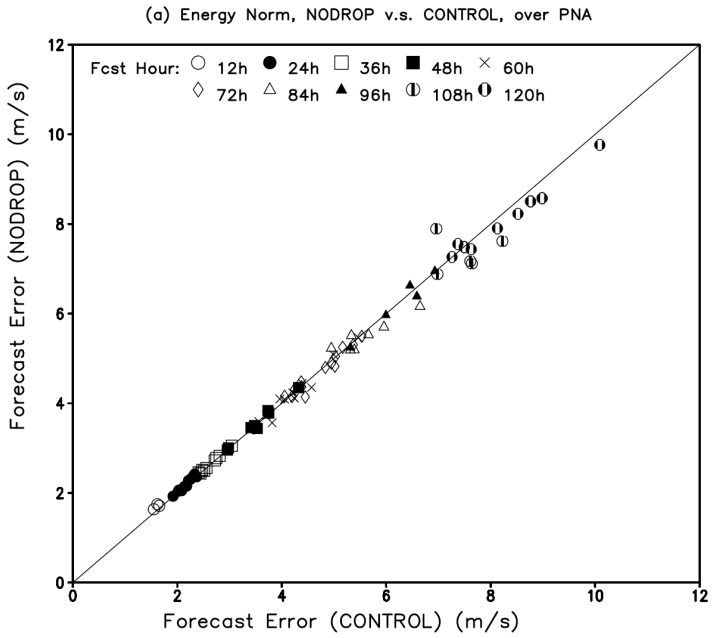

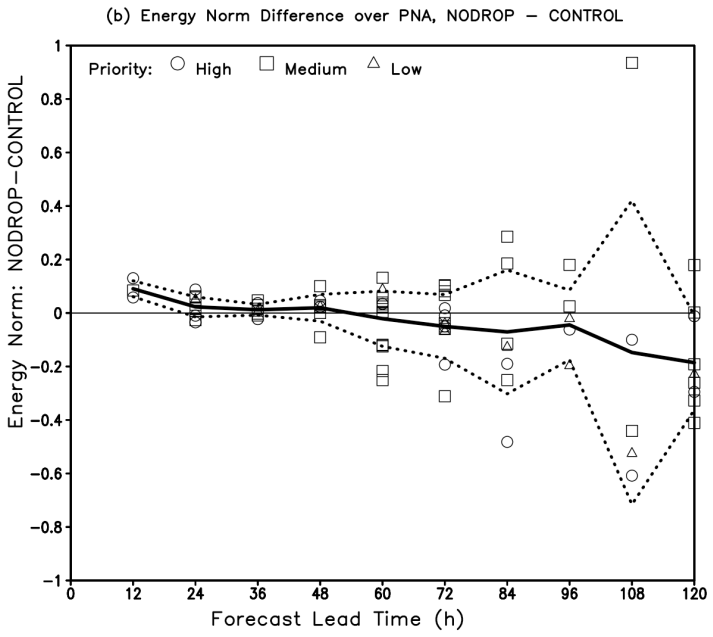

Figure 3: As in Fig. 2, but for the PNA region (20° N - 75° N, 180° E - 320° E).

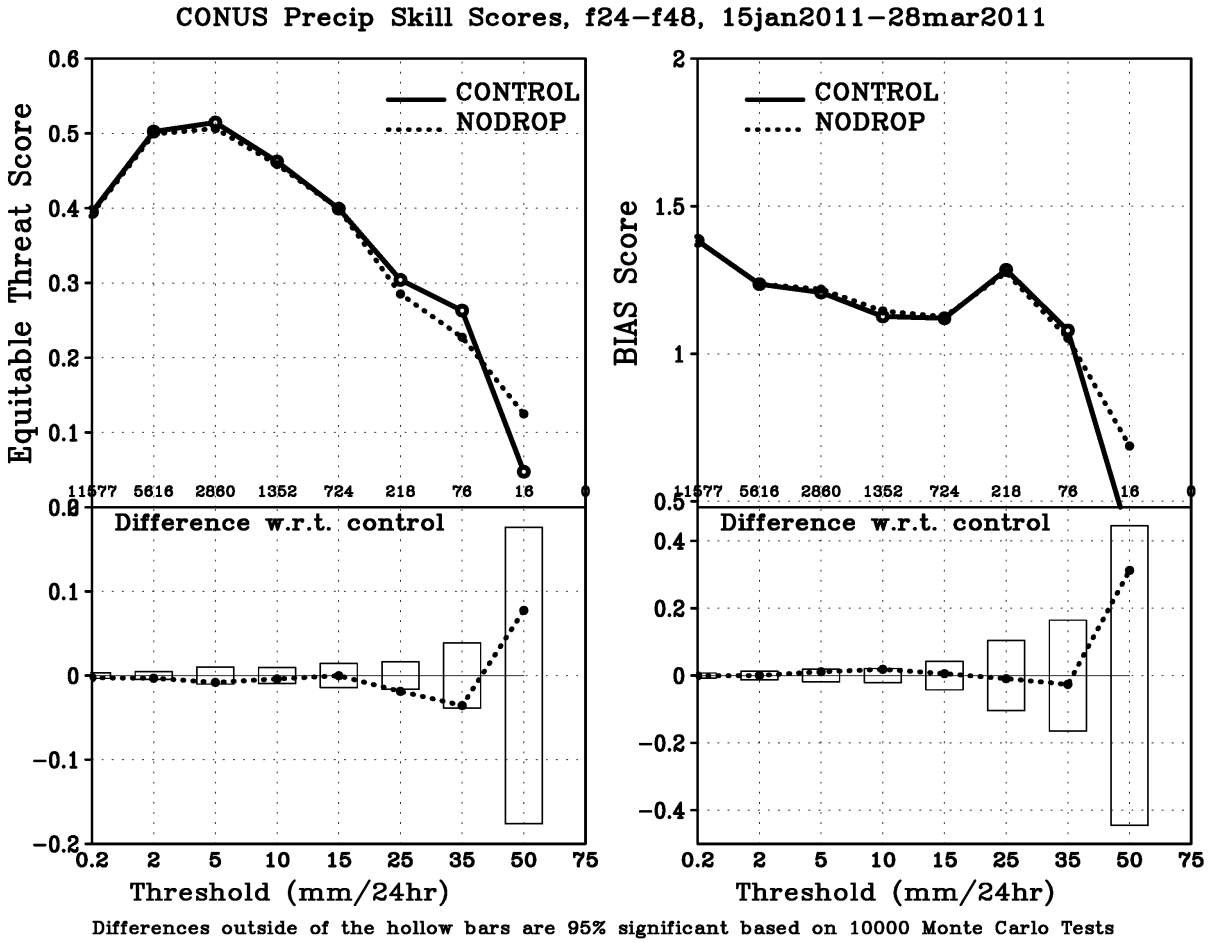

Figure 4: Equitable threat score and bias score for 24-hour accumulated precipitation from forecast hours +24 to +48 verified over the contiguous US. Top panels provide the scores, and bottom panels provide the difference (solid lines) between the NODROP and CONTROL experiments and 95% confidence intervals (bars) based on 1000 realizations of Monte-Carlo tests.

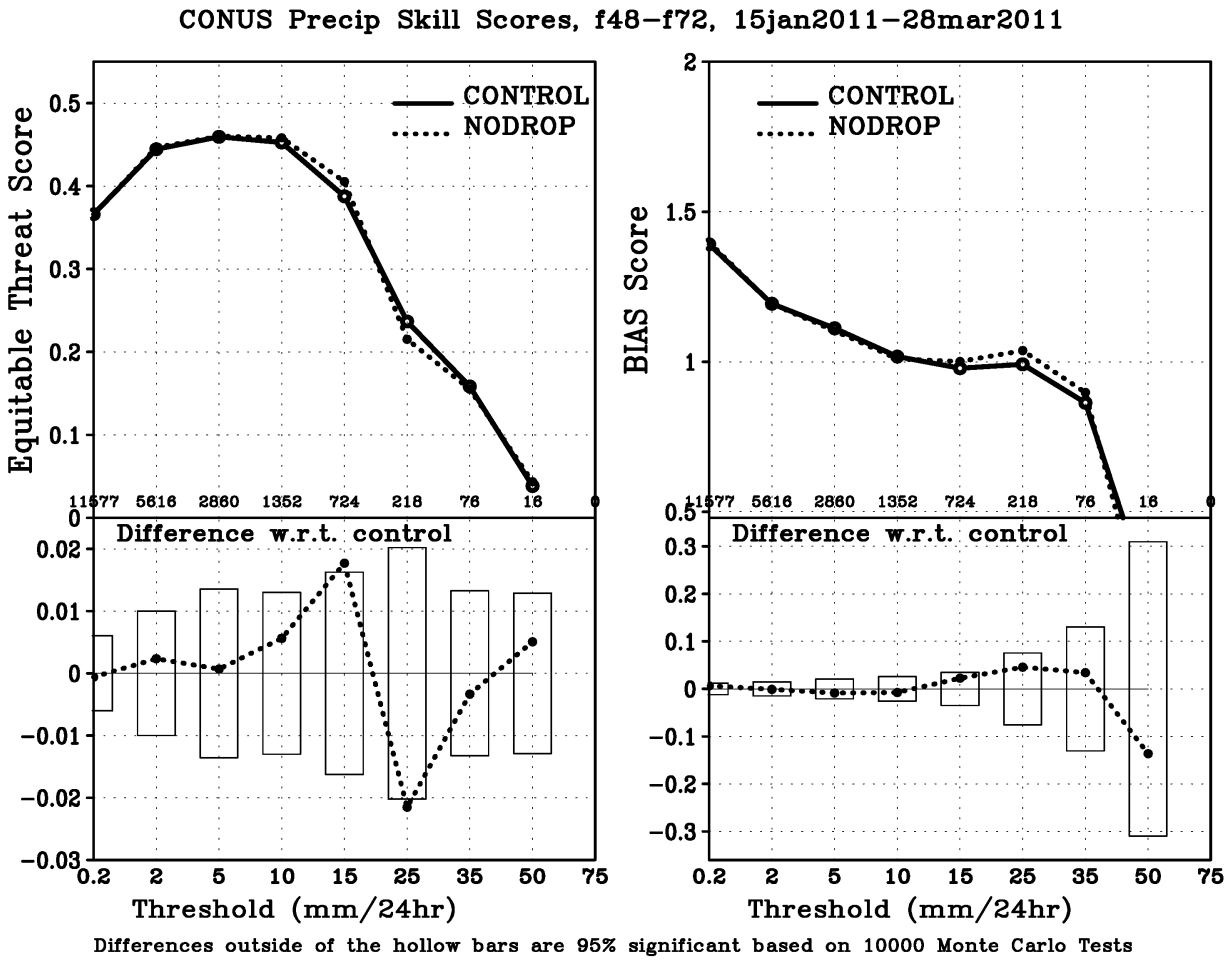

Figure 5: As in Fig. 4, but for 24-hour accumulated precipitation from forecast hours +48 to +72.